Earth and Planetary Science Letters 503 (2018) 216–226

Contents lists available at ScienceDirect

Earth and Planetary Science Letters

www.elsevier.com/locate/epsl

Geodetic measurements reveal short-term changes of glacial mass near Jakobshavn Isbræ (Greenland) from 2007 to 2017

Bao Zhang [a,b,*], Enze Zhang [a], Lin Liu [a], Shfaqat Abbas Khan [c], Tonie van Dam [d], Yibin Yao [b], Michael Bevis [e], Veit Helm [f]

[a] Earth System Science Programme, Faculty of Science, The Chinese University of Hong Kong, Hong Kong, China
[b] School of Geodesy and Geomatics, Wuhan University, Wuhan 430079, China
[c] DTU Space-National Space Institute, Technical University of Denmark, Department of Geodesy, Kgs. Lyngby, Denmark
[d] Faculty of Science, Technology, and Communication, University of Luxembourg, Luxembourg City, Luxembourg
[e] School of Earth Sciences, Ohio State University, Columbus, OH, USA
[f] Glaciology Section, Alfred Wegener Institute, Helmholtz Centre for Polar and Marine Research, Bremerhaven, Germany

ARTICLE INFO

Article history:
Received 19 June 2018
Received in revised form 23 September 2018
Accepted 25 September 2018
Available online 9 October 2018
Editor: R. Bendick

Keywords:
Jakobshavn Isbræ
geodetic measurements
short-term ice mass change
dynamic thickening

ABSTRACT

The Global Positioning System (GPS) and Gravity Recovery and Climate Experiment (GRACE) provide important geodetic datasets to study glacial mass change. Applying the multichannel singular spectral analysis to the GPS-measured vertical and horizonal crustal displacement and GRACE-derived vertical displacement near Jakobshavn Isbræ (JI) in western Greenland from 2007 to 2017, we reconstruct the short-term loading displacements due to ice mass changes. Both the vertical and east displacements show strong seasonal variability. They also reveal three episodes of transient displacements: downward and eastward motion from late 2007 to around 2010, sustained upward and westward motion from 2010 to early 2013, and downward and eastward motion till late 2016. We also forward model the seasonal and transient displacements caused by surface mass balance (SMB) and glacier dynamics. Our model agrees well with the geodetic observations and provides quantitative insights into the contribution from SMB and ice dynamics to the ice mass changes. We find that SMB is the dominant contributor to the seasonal and transient displacements at three out of four GPS sites (AASI, ILUL, and QEQE). While, at the fourth GPS site (KAGA) that is closest to the glacier, the contributions to the transient displacements from SMB and glacier dynamics are comparable. The forward modeling also suggests that the dynamic mass change in the JI catchment underwent strong seasonal variations and these variations correlated more with the seasonal retreat and advance of the calving front than with the changes of glacial velocities. Our altimetry results reveal that the frontal portion of JI catchment lost 34 Gt in 2012 and this loss of ice declined to only 11 Gt in 2016 due to widespread thickening along the main flowline.

© 2018 Elsevier B.V. All rights reserved.

1. Introduction

Jakobshavn Isbræ is the largest and fastest outlet glacier on the west coast of Greenland, draining ~6.5% of the ice sheet before 2000 (Krabill et al., 2000). JI changed dramatically from 1998 to 2003, during when it doubled the moving speed as its ~15 km long floating ice tongue disintegrated (Thomas et al., 2003; Joughin et al., 2004). The ice mass loss rate in the JI catchment reached near 25 Gt a^{-1} by the end of 2002 and then stabilized and declined back under 20 Gt a^{-1} until 2006. It increased to 34 Gt a^{-1} by the end of 2007, and afterwards the ice mass loss rate fluctuated between 25 and 33 Gt a^{-1} (Howat et al., 2011).

JI showed a sudden acceleration in thinning and velocity in 1997, which was triggered by warm subsurface ocean water (Holland et al., 2008). At almost the same time, the JI catchment turned from slow thickening to sustained thinning (Thomas et al., 2003; Holland et al., 2008). Joughin et al. (2014) found that the mean annual speed of a point on JI for 2012 was about three times as that in the mid-1990s. Two severe melting events occurred in 2010 and 2012 (Tedesco et al., 2011; Nghiem et al., 2012), which temporally accelerated the ice mass loss in JI.

Ice discharge and calving front retreat are the two main contributors to JI's dynamic mass loss. Cassotto et al. (2015) pointed

* Corresponding author at: School of Geodesy and Geomatics, Wuhan University, Wuhan 430079, China.
E-mail addresses: sggzb@whu.edu.cn (B. Zhang), liulin@cuhk.edu.hk (L. Liu), abbas@space.dtu.dk (S.A. Khan), tonie.vandam@uni.lu (T. van Dam), mbevis@osu.edu (M. Bevis), veit.helm@awi.de (V. Helm).

https://doi.org/10.1016/j.epsl.2018.09.029
0012-821X/© 2018 Elsevier B.V. All rights reserved.

out that seasonal variations in calving influence a glacier's long-term rate of retreat through nonlinear processes (Amundson and Truffer, 2010; Joughin et al., 2012). Simulations carried out by Muresan et al. (2016) also showed that the changes of JI horizontal velocities are a response to variations in terminus position. Bondzio et al. (2017) investigated the mechanisms causing widespread flow acceleration of JI using a three-dimensional model and found that the calving front position is the dominant control.

These studies indicate that the glacial mass loss is far from a steady process and variations in surface mass balance (SMB), ice discharge, and calving front positions can significantly influence the short-term variation of JI's ice mass balance. However, there is still a lack of detailed and quantitative analysis on the seasonal and transient (inter-annual) mass changes caused by SMB, ice discharge, and calving font positions at or near JI.

Currently, more than 50 continuously-operating Global Positioning System (GPS) receivers are deployed around the edge of the Greenland Ice Sheet, most of which are part of the Greenland network (GNET). These GPS sites provide important geodetic data that records the crust's response to historical/present ice mass changes. Previous studies have used GPS measurements of vertical crustal movements to study the present-day glacial mass change (Khan et al., 2010a; Bevis et al., 2012; Nielsen et al., 2013; Adhikari et al., 2017; Kjeldsen et al., 2017) or to constrain the glacial isostatic adjustment (GIA) signal (King et al., 2010; Khan et al., 2016). However, most of these studies focused on the long-term changes of glacial mass and few of them have addressed the transient and seasonal variations and the interaction between them. Zhang et al. (2017) combined the GPS- and GRACE-derived vertical displacements to mitigate the negative impacts of colored noise in GPS data and the low sensitivity of GRACE data to outlet glaciers and successfully detected and identified the transient ice mass changes in Upernavik Isstrøm, another Greenland outlet glacier located 450 km north of JI.

In this study, we aim to (1) characterize the seasonal and transient variations of the ice mass changes in the JI catchment, and to (2) partition individual contributions from SMB, ice discharge, calving front positions, and their sum. We use both GPS vertical and horizontal displacements and GRACE-derived vertical displacements to reconstruct the seasonal and transient signals using the multichannel singular spectral analysis (M-SSA) (Sections 2 and 3). We forward model the seasonal and transient displacements due to SMB, ice discharge, and calving front position changes (Section 4). We compare the seasonal and transient displacements from observations and models and present the ice thickness change using altimetry data (Section 5). The forward model offers quantitative insights into the seasonal and transient mass variations caused by SMB, ice discharge, and calving front retreat (Section 6). Compared with Zhang et al. (2017), this work is new in three aspects. First, the east component of GPS position time series is successfully used to detect the seasonal and transient signals. Second, the seasonal and transient mass loss caused by ice discharge and calving front changes are quantified separately. Third, we use the altimetry data and find the widespread thickening near the glacier's frontal portion from April 2016 to April 2017, which never happened in the previous decade. In addition to the above innovations, this study uses multi-source geodetic data (GPS, GRACE, altimetry, and Synthetic Aperture Radar) to reveal the ice mass changes from different perspectives, providing us a comprehensive knowledge of the highly-dynamic mass variations of JI.

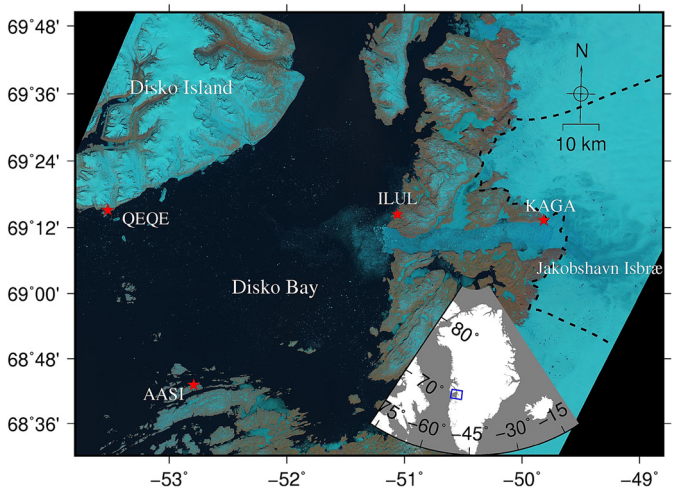

Fig. 1. Map of the study area. The background is a Landsat-8 image taken on May 31st, 2017. The red stars show the locations of the four GPS sites. The black dashed lines mark the JI catchment.

2. Geodetic data analysis

2.1. GPS data

As part of the GNET, four GPS sites were deployed near JI and on Disko Island in 2005 and 2006 (Fig. 1). Among them, KAGA is the closest to the glacier, which is only ∼6 km downstream from the calving front of JI on May 31, 2017; while ILUL, AASI, and QEQE are ∼56 km, ∼136 km, and ∼150 km from the calving front, respectively. The different sensitivities of the 4 sites to JI's mass change help to infer the approximate location of the mass change (Khan et al., 2010a; Wahr et al., 2013) and will also be beneficial for signal extracting.

The GPS data from April 2007 to April 2017 are processed by the same software and strategies as detailed in Khan et al. (2010a) and Liu et al. (2017). Data before 2007.4 at KAGA were bad in quality and thus are not used. At each site, we obtain time series of daily position solutions and their uncertainties in the local north, east, and up directions in the International Global Navigation Satellite System Service 2008 (IGS08) frame. Since we focus on the short-term displacements caused by ice loading changes, we first remove the trend and non-ice loadings from both the vertical and horizontal displacements. The technical details and the detrended time series can be found in Section S1 of the Supplementary Material (SM).

2.2. Vertical displacements derived from GRACE

We calculate the bedrock vertical displacements due to surface mass loading using the GRACE gravity data. The idea is to convert the time-varying gravitation fields to the vertical displacements using the load Love numbers (van Dam et al., 2007). We use the most recent release (RL06) of the GRACE GSM products (Level-2) from the Center for Space Research (CSR), University of Texas Austin. The CSR GSM products contain spherical harmonic coefficients up to degree 60 for each monthly gravity field. We include the degree-1 coefficients from Swenson et al. (2008) and use the monthly degree-2 order-0 coefficients from satellite laser ranging products provided by Cheng et al. (2013). These products have already removed the mass contributions from ocean and atmosphere. We further remove the continental water storage changes from the GSM products using the Noah land hydrology model in the Global Land Data Assimilation System (Rodell et al., 2004). The remain gravity changes are due to ice mass changes and GIA.

We calculate the uplift dr of the Earth's bedrock at latitude θ and longitude φ using the following equation, same as equation (2) of van Dam et al. (2007):

$$dr(\theta,\varphi) = R\sum_{l=0}^{l=60}\sum_{m=0}^{m=l} W_l \tilde{P}_{lm}(\cos\theta)\left(C_{lm}\cos(m\varphi) + S_{lm}\sin(m\varphi)\right) \times \frac{h'_l}{1+k'_l} \quad (1)$$

where R is the Earth's radius, l and m are degree and order numbers, $\tilde{P}_{lm}$ are normalized associated Legendre functions, W_l is the weighting function, h'_l and k'_l are the load Love numbers from Han and Wahr (1995), and C_{lm} and S_{lm} are the GSM spherical harmonic coefficients. We apply a Gaussian smoothing kernel of 300 km radius.

We fit and remove the linear and quadratic terms from the GRACE-derived uplift time series to remove long-term changes (including GIA). We refer to the detrended GRACE-derived vertical displacements as the "GRACE data" hereinafter. Since the GRACE-inferred horizontal displacements have very small magnitude and low signal-to-noise ratio, we do not use them in this study. These GRACE data will be used to validate the GPS signals due to ice mass changes and to reinforce our confidence in the extracted signals.

2.3. Altimetry data

We estimate the rate of ice volume change using 2006–2017 NASA's Airborne Topographic Mapper (ATM) flights (Krabill, 2017) derived altimetry, supplemented with laser altimetry observations from the Ice, Cloud and land Elevation Satellite (ICESat) (Zwally et al., 2012) for 2006–2009 and radar altimetry from the CryoSat-2 satellite (Helm et al., 2014) for 2010–2017. Taking firn compaction into account, we convert the volume loss rate into a mass loss rate using the method described by Kuipers Munneke et al. (2015). Then we integrate the mass change rates to obtain mass changes referenced to April 2006. To predict the elastic displacements, we convolve the mass change estimates (from ICESat, ATM, and CryoSat-2) with the loading Green's functions for vertical displacements (Farrell, 1972). We obtain the transient mass changes and bedrock displacements by removing the linear and quadratic terms.

3. Extracting transient and seasonal signals

In this section, we describe how we extract transient and seasonal signals from the GPS and GRACE data using M-SSA and test the significance of the extracted signals using Monte-Carlo SSA (MC-SSA). M-SSA can decompose the complex time series into simple components, such as trends, transients, oscillations, and noise. The data-adaptive nature of M-SSA makes it suitable for extracting seasonal signals with time-varying amplitudes and phases and irregular transient signals. MC-SSA can help identify signals from colored noise. The combined use of M-SSA and MC-SSA has been proven to be an effective way to extract signals from noisy GPS and GRACE time series (Ghil et al., 2002; Rangelova et al., 2010, 2012; Chen et al., 2013; Walwer et al., 2016; Zhang et al., 2017).

3.1. GPS signals

After post-processing the GPS data, we obtain 3,653 common daily data points spanning from 2007.4 to 2017.4. We follow Zhang et al. (2017) to apply M-SSA with a window width of 700 days to the north, east and up time series, respectively. The first 10 decomposed components are shown in Fig. S2 of the SM, among which the first 6 components contain the seasonal and transient signals.

We perform the MC-SSA to identify signals from colored noise. The testing results show that among the first 6 components, only the first eigenvalue of the north components lies inside the confidence interval, indicating this component is colored noise (Fig. S3 of the SM). Since the ice mass is mainly located on the east side of the 4 sites and the mass changes in the north and south have a canceling effect on loading displacement, the displacements in the north direction have a smaller signal-to-noise ratio than the east and up displacements. Consequently, the GPS results from the north components fail to pass the MC-SSA test and will not be used. The first 6 components in the east and up directions lie above the corresponding confidence intervals, indicating they are not colored noise. Based on the results shown in Fig. S2 of the SM, we reconstruct the transient and seasonal signals in the east and up directions (see more in Section S1 of the SM).

3.2. GRACE signals

GRACE has a spatial resolution of about ~330 km, whereas all 4 GPS stations studied here would fit inside of a circle with a radius <100 km. The smoothed or blurry mass change solutions produced by GRACE do not accurately characterize the mass losses associated with retreat and thinning of Jakobshavn glacier. As a result, the vertical displacements predicted using GRACE's mass change fields are very similar at all four GPS stations. Therefore, we only apply M-SSA to the GRACE data at KAGA with a window width of 25 months. Since the GRACE data are free of colored noise, MC-SSA is not performed. The first 10 decomposed components are shown in Fig. S4 of the SM.

4. Forward modeling

4.1. Loading due to SMB

Using the simulated SMB of Greenland from the regional climate MAR model (version 3.8, Fettweis et al., 2017 updated in 2018) that is convolved with the loading Green's functions, we calculate the vertical and horizontal displacements caused by the SMB changes. As the MAR outputs are monthly increments, we first integrate the SMB-estimated displacements and then fit and remove the linear and quadratic terms from it. We refer to the residual displacements as the "SMB data" hereinafter.

Finally, we apply M-SSA to the SMB data at the 4 sites and reconstruct the seasonal and transient signals using the same methods as described in Section 3. Since the SMB data are simulated results, MC-SSA test is unnecessary.

4.2. Loading due to glacier dynamics

To quantify the ice discharge from the JI catchment, we perform a fluxgate calculation similar to Rignot and Kanagaratnam (2006). We use the glacial surface velocity maps produced by Joughin et al. (2010, updated in 2016) using Synthetic Aperture Radar offset tracking from 2009 to 2015. We extend the temporal coverage back to 2007 by using surface velocity maps from optical images (Ahn and Howat, 2011; Jeong and Howat, 2015; Jeong et al., 2017). As an example, Fig. 2 shows the mean velocity between April 1 and April 12, 2014. According to our practice, when the fluxgate is closer to the terminus, the result will be better. Therefore, we set the fluxgate as close to the terminus as possible and meanwhile ensure there are no velocity data gaps along the fluxgate.

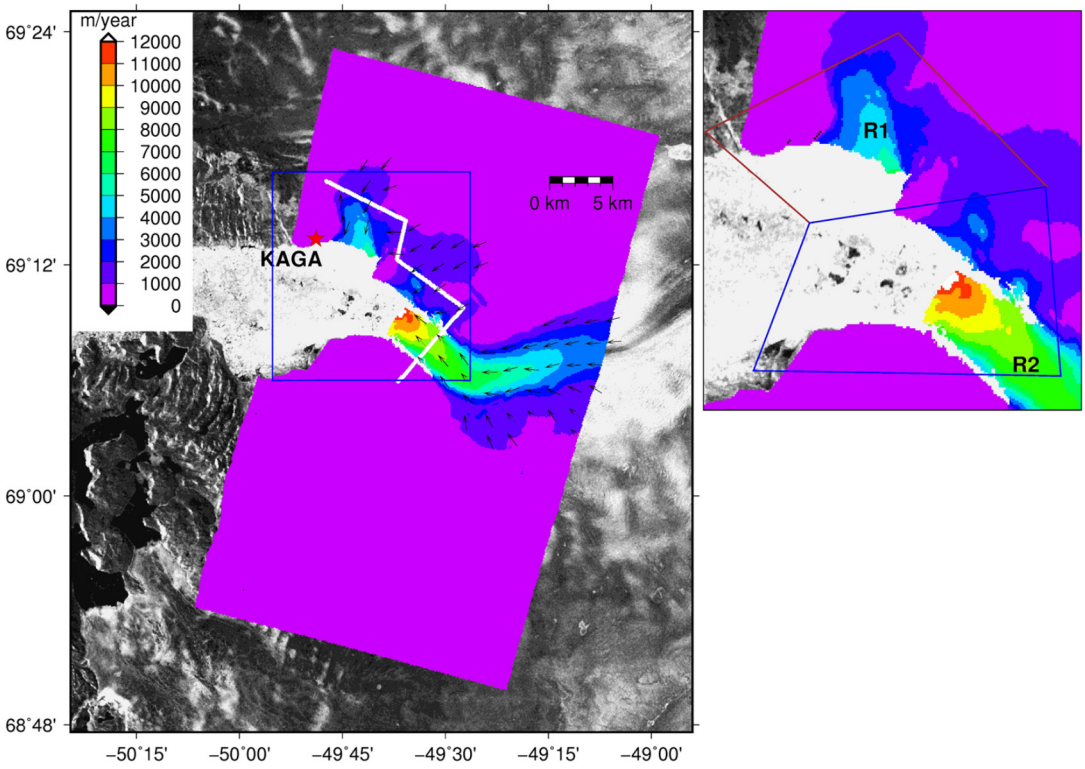

Fig. 2. Map of mean ice velocity between April 1 and April 12, 2014 (based on Joughin et al., 2010, updated in 2016). The white lines mark the fluxgate we use for calculating dynamic mass changes. The black lines define the downstream and upstream of the fluxgate. The arrows indicate the velocity directions. The red star indicates the GPS site KAGA. The right figure shows the downstream of the fluxgate as marked by the blue rectangle in the left figure. We divide the downstream of the fluxgate into two sub-regions (labeled as 'R1' and 'R2') according to the two main channels. (For interpretation of the colors in the figure(s), the reader is referred to the web version of this article.)

Knowing the surface ice velocity $\mathbf{V}$ and ice thickness H along a fluxgate with a width W, we calculate the rate of ice mass passing through the fluxgate, denoted as $\dot{m}_{Dyn}$ by performing the following integral

$$\dot{m}_{Dyn}(t) = \rho \int_0^W H\big(\mathbf{V}(t)\cdot\mathbf{n}\big)dw \tag{2}$$

where ρ is the ice density, set as a constant of 913 kg/m^3 since the study area is located in the ablation zone, dw is the incremental width along the fluxgate, $\mathbf{n}$ is the unit normal vector directed outward from the fluxgate, t is the time. We use the ice thickness map provided by Morlighem et al. (2017). We ignore any temporal changes of the ice thickness along the fluxgate. Using this method, we estimate the ice discharge rate from the upstream of the fluxgate. The only time-varying parameter in Eq. (2) is the surface velocity. Bamber et al. (2000) showed depth-averaged and surface velocities are nearly identical over JI. Rignot et al. (2008) also claimed that using surface velocity to represent the depth-averaged velocity only overestimates ice velocity by 1–2% near the coast. Therefore, we use the surface velocity to represent the depth-averaged velocity.

Since the SMB changes are negligible downstream of the fluxgate according to the MAR model, the mass changes in the downstream are mainly caused by glacier dynamics. To account for the dynamic ice mass change downstream of the fluxgate, we calculate the volume mass change caused by the calving front changes as the product of the area change and ice thickness. The calving fronts are obtained from the Environmental Earth Observation Greenland Calving Front Dataset 1990–2016 (version 2.0, http://cryoportal.enveo.at). We choose the calving front location on March 8, 2007 as the reference and take the area between any selected calving front and the reference as the area change. Due to a lack of ice thickness data downstream of the fluxgate, we divide the region downstream of the fluxgate into two sub-regions (R1 and R2, as shown in Fig. 2) and use constant average ice thicknesses of 187 m and 720 m for R1 and R2, respectively. It should be noted that not all the lost ice in the downstream will cause loading change since seawater will refill where the ice was lost. Only the ice above the floating height of hydrostatic equilibrium will cause loading changes. Its thickness is calculated by

$$T_h = H - (H - e_s)\times\frac{\rho_{sw}}{\rho} \tag{3}$$

where T_h is the ice thickness above the floating height, e_s is the ice surface elevation, ρ_{sw} is the seawater density (1050 kg/m^3). The average surface elevations for R1 and R2 are 165 m and 197 m. Finally, we obtain T_h as 161 m and 119 m for R1 and R2, respectively. By the above assumptions, the calving front change is the only variable in the calculation of ice mass change downstream of the fluxgate.

The GPS-measured loading displacements caused by mass changes are determined not only by the magnitude of mass changes but also by their spatial distribution with respect to the GPS sites. By the fluxgate calculation described above, we have obtained the ice discharge rates in the upstream of the fluxgate. By considering the ice volume change, we have calculated the mass loss in the downstream of the fluxgate. Next, we use a data-driven approach to distribute them spatially. The idea is to distribute the total ice mass loss over the JI catchment according to ice elevation changes caused by glacier dynamics. Below we describe how we distribute the ice discharge rates from the upstream. The same method is also applied to the mass loss from the downstream.

To account for the temporal variations of dynamic ice mass loss, we first integrate the altimetry-derived yearly elevation changes (Section 2.3) over time to obtain cumulative elevation changes. We then resample them to monthly intervals by the spline interpolation. Such interpolation mitigates abrupt jumps and gives more realistic results than simply using the yearly elevation changes. We further remove the elevation change caused by SMB from the total elevation change to obtain the elevation change caused by glacier dynamics, denoted as dh. Assuming that the dynamic mass loss rate dm_i at any point i within the drainage basin is proportional to dh_i, we can calculate dm_i as

$$dm_i = \frac{dh_i}{\sum_{j=1}^{n} dh_j} \dot{m}_{Dyn} \tag{4}$$

where n is the total number of points within the drainage basin. We use this equation to distribute the total ice discharge. Next, we convolve dm_i with the loading Green's functions to retrieve bedrock displacement rates at the four GPS sites. We integrate the displacement rates to obtain the displacements at each site. Then we fit and remove the linear and quadratic terms from each displacement time series. Finally, we apply M-SSA to the detrended displacement time series and reconstruct the seasonal and transient signals.

5. Results and comparisons

5.1. Comparing observations with forward models

Figs. 3a–3h compare the extracted seasonal signals from our modeling results and observations. Overall, the seasonal signals extracted from SMB, GPS, and GRACE show strong similarities in phases and amplitudes. But the seasonal signals due to glacier dynamics have much smaller amplitudes than those derived from SMB, GPS, and GRACE at three (AASI, ILUL, and QEQE) of the four sites. This indicates that the seasonal displacements are mainly caused by SMB with much smaller contribution from glacier dynamics at these three sites. At KAGA, the seasonal signal due to glacier dynamics has a much larger amplitude than those at the other three sites. This is due to the short distance between KAGA and the calving front. Figs. 3a–3h also show that the seasonal signals in the east direction are much smaller than those in the up direction. This is because the horizontal elastic response of the bedrock to loading change is not as sensitive as the vertical response (Wahr et al., 2013) and thus more vulnerable to outliers and noise. This can also explain why the east signals are not modeled as well as the vertical signals.

We also note a few disagreements between the observations and the forward models. First, the amplitude of the GRACE seasonal signal is apparently smaller than the GPS signal at KAGA in the up direction. Such discrepancy is due to the low sensitivity of GRACE to local dynamic mass change (Khan et al., 2010b). Second, the GPS seasonal signals tend to be underestimated compared with the GRACE and SMB signals. This is because that the outliers in GPS position time series have a strong influence on the extraction of the seasonal signals and we use only the most reliable components to reconstruct the seasonal signals.

Figs. 3i–3l compare the extracted transient signals from observations and models in the up direction. The transient signals extracted from GPS, GRACE, and SMB show similar varying patterns at AASI, ILUL, and QEQE. This pattern is characterized by a subsidence from late 2007 to early 2010 and an uplift from early 2010 to early 2013 and then a subsiding trend till late 2016. The transient signals due to glacier dynamics show different phases from the other signals. The GPS transient signals are different in amplitudes and phases from the GRACE and SMB transient signals at KAGA. This is because that the loading displacements at KAGA are much influenced by the glacier dynamics, while the GRACE signals are insensitive to glacier dynamics and SMB is free of it. Glacier dynamics caused relatively small vertical displacements at AASI, ILUL, and QEQE, due to their long distances from JI.

In Figs. 3m–3p, the east transient signals from GPS and SMB showed consistent varying patterns at the 4 sites. They all moved eastward before early 2010, then westward till early 2013, and then eastward again. The timings of these changes were consistent with those in the up direction. However, the transient signals extracted from glacier dynamics show different varying patterns from the GPS and SMB transient signals. This reflects asynchronous variations between SMB and glacier dynamics.

According to the elastic loading theory (Farrell, 1972; Wahr et al., 2013), when a mass load decreases, the site will uplift and move away from the load. Conversely, if the load increases, the site will subside and move toward it. Therefore, the displacements shown in Figs. 3i–3p reveal that there was less-than-normal ice mass loss before 2010, more-than-normal ice mass loss from 2010 to the end of 2012, and less ice mass loss since then, and most of the ice mass changes occurred east to the 4 sites.

Fig. 4 shows the comparisons among the GPS, GRACE, and the modeled seasonal and transient displacements in forms of the sum of the SMB and glacier dynamics components. Both the seasonal and transient signals from the observations agree well with those from the forward modeling in the up direction (Figs. 4a–4d, 4i–4l). The transient signals derived from the GPS data and forward modeling are moderately consistent in the east direction (Figs. 4m–4p). But, in the east direction, the modeled seasonal signals tend to be larger than the GPS signals (Figs. 4e–4h). This is mainly due to the underestimation of the seasonal signals from the GPS data.

5.2. Short-term ice mass changes and bedrock displacements inferred from altimetry data

Altimetry data we have only cover JI's frontal portion. The area with altimetry data available is marked as the near-field area and the area outside is marked as the far-field area. Fig. 5 shows the transient mass changes and bedrock displacement inferred from the altimetry-derived ice elevation changes near the frontal portion, in comparison with the GPS transient signal at KAGA. We have removed the far-field SMB contributions from the GPS transient signal. Therefore, the transient signals derived from GPS and altimetry are generated from the same near-field area. The transient vertical displacements inferred from the altimetry data are consistent with the GPS results. The transient east displacements inferred from the altimetry data also agree with the GPS-inferred displacement though not as well as the vertical component. These agreements reinforced our confidence in the extracted transient signals. Fig. 6 shows that JI's frontal portion kept thinning from 2006 to 2016 and reached the maximum annual thinning in 2012 by losing 34 Gt. However, from April 2016 to April 2017, the ice elevation near the front increased by up to 3 m. Such ice thickening never happened in the previous decade. Due to such widespread thickening, the frontal portion lost only 11 Gt of ice mass from April 2016 to April 2017.

6. Discussion

6.1. Short-term mass changes caused by SMB, ice discharge, and migration of calving front

The transient displacements were caused by transient changes in SMB, ice discharge, and migration of calving front. Section S5 of the SM shows that the cumulative uplifts in ablation season

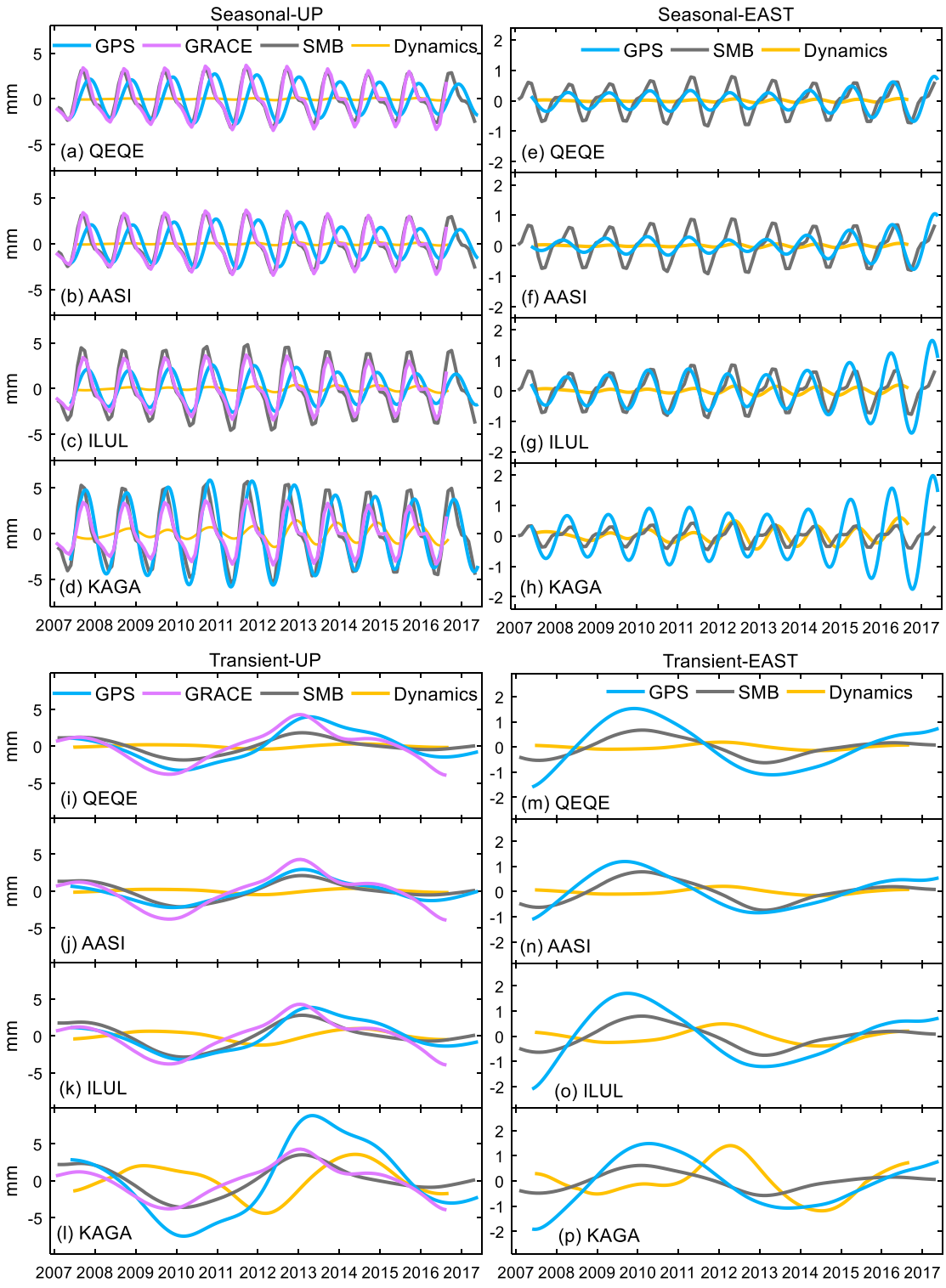

Fig. 3. Reconstructed seasonal and transient signals derived from GPS, GRACE, SMB, and glacier dynamics.

were more variant than the cumulative subsidence in accumulation season, suggesting that the transient SMB changes were mainly caused by abnormal ablation with little contribution from abnormal accumulation. Then, we separately analyze the dynamic mass loss from the downstream and upstream of the fluxgate. We find that (1) the transient ice mass loss from the upstream was much more variant than that from the downstream (Fig. 7a); and (2) the dynamic mass loss from both upstream and downstream underwent seasonal oscillations with stronger amplitudes in the downstream than in the upstream (Fig. 7b). This indicates that the transient signals were mainly caused by the inter-annual variations of the ice discharge while the seasonal signals were largely influenced by the seasonal retreat and advance of the calving front. The amplitudes of the seasonal mass loss in the downstream varied with time: showing a decreasing trend from 2007 to 2010 and remaining nearly constant after 2011. The amplitudes of the seasonal mass loss in the upstream were smaller before 2011 and larger after that. These changes suggest that the seasonal dynamic mass

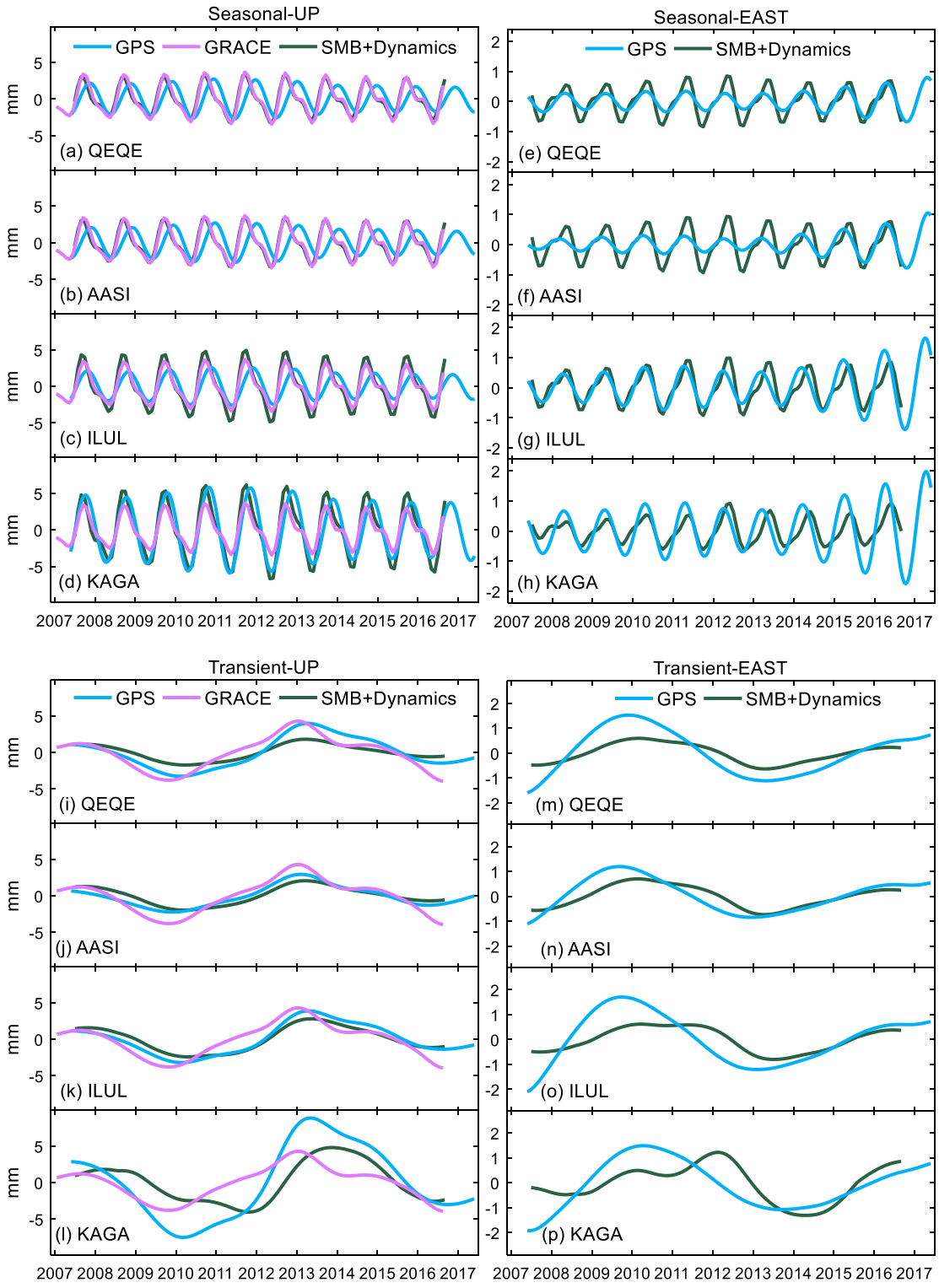

Fig. 4. Reconstructed seasonal and transient signals derived from GPS, GRACE, and SMB plus glacier dynamics.

loss in JI had different temporal behaviors before and after 2010. We also observe a phase shift between the seasonal mass loss of the upstream and downstream after 2010, i.e., the seasonal mass loss of the downstream peaked earlier than that of the upstream. This suggests that the seasonal variation of the ice discharge may be a delayed response to the calving front change.

Fig. S5 of the SM shows the calving front positions from 2007 to 2016. It suggests that the significant retreat happened in 2012 and 2014, coincident with the accelerated mass loss of the upstream as shown in Fig. 7a. The significant advance happened in 2011 and 2015, coincident with the decelerated mass loss as shown in Fig. 7a. This suggests that the calving front position change has a strong influence on the ice discharge of JI. Amundson et al. (2008) also showed the speedup of JI is coincident with terminus retreat. Simulations carried out by Muresan et al. (2016) and model results from Bondzio et al. (2017) also showed that the calving front

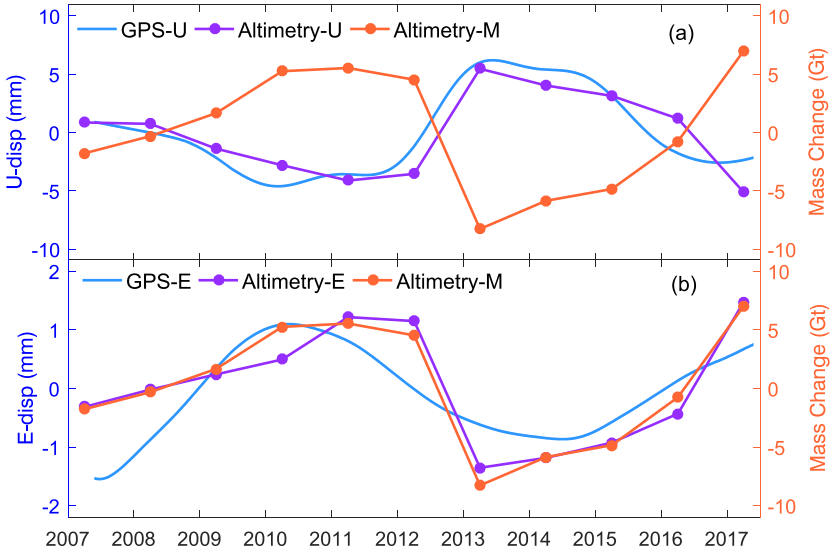

Fig. 5. Transient vertical ('Altimetry-U') and east ('Altimetry-E') bedrock displacements at KAGA and transient mass changes ('Altimetry-M'), both inferred from the altimetry data near JI. 'GPS-U' and 'GPS-E' are the GPS-estimated transient vertical and east displacements at KAGA after removing the far-field SMB contributions.

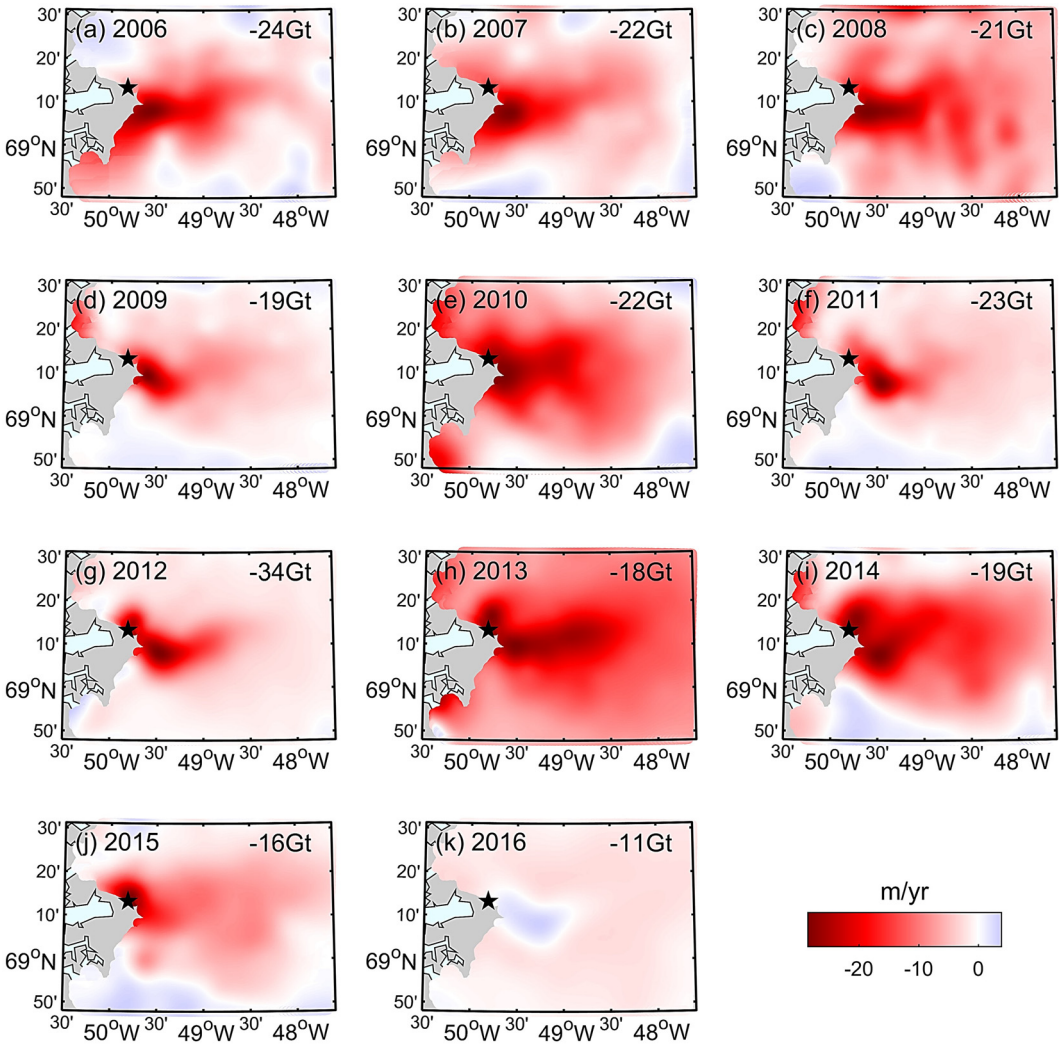

Fig. 6. Annual (April to April) ice elevation changes near JI's frontal portion from 2006 to 2017, derived from altimetry measurements. Negative values mean thinning. The black star marks the location of KAGA. The number in the top right corner of each panel indicates the annual ice mass change.

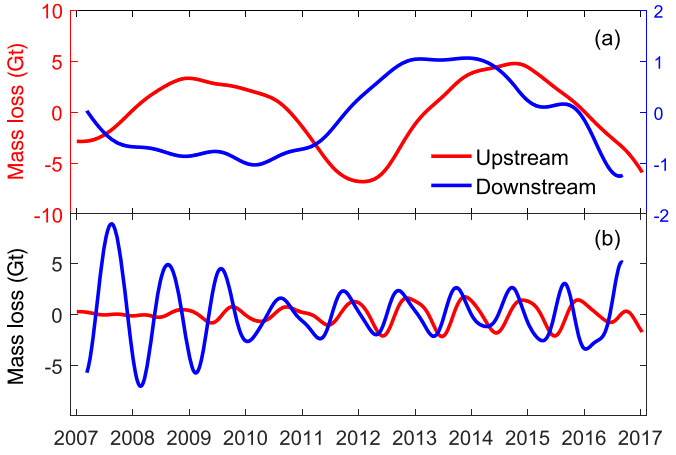

Fig. 7. Transient (a) and seasonal (b) dynamic ice mass loss from the JI catchment. The red and blue lines indicate the dynamic ice mass loss from the upstream and downstream of the fluxgate, respectively.

position had a dominant influence on changes of JI horizontal velocities. The relationship between JI's calving front position and horizontal velocities can be explained by that when JI terminus retreats, the glacier speeds up to increase strain rate dependent resistive stresses upstream to compensate for the loss of downstream contact with the bed and/or fjord walls (Joughin et al., 2012).

Although we have partitioned the seasonal and transient dynamic ice mass change from both upstream and downstream of the fluxgate, the method still suffers from a few limitations. First, in the fluxgate calculation, we use constant thickness along the fluxgate. According to the altimetry data, the ice surface elevation close to the center of the fluxgate (where the thickness is ~1400 m) dropped by more than 100 m from 2007 to 2015. Ignoring such changes in ice thickness can cause as much as ~7% estimation error. Second, the time interval of the calving front position product is ~3 months and the ice thickness near the calving front is assumed to be time-invariant. These may bias the estimation of the mass change downstream of the fluxgate. Third, the elevation changes derived from the altimetry data have a temporal resolution of 1 year, which cannot reflect the seasonal variations and thus influences the mass distribution and loading displacement calculation.

6.2. Dynamic thickening in 2016

To investigate what caused the widespread thickening between April 2016 and April 2017, we calculate the SMB induced elevation changes and dynamic induced elevation changes, respectively. Since the SMB data have a resolution of 5 km and the altimetry data have a resolution of 250 m, we interpolate the altimetry data to the SMB data grid and then remove the SMB induced ice elevation changes from the altimetry data to obtain the dynamically induced ice elevation changes. Fig. 8a shows that the SMB did not cause any thickening during April 2016 and April 2017. By contrast, Fig. 8b shows that the glacier dynamics caused apparent thickening near the frontal portion, which is very similar to the elevation change as shown in Fig. 6k. This agreement indicates that the widespread thickening in 2016–2017 was caused by glacier dynamics: a decrease of ice flow velocity near the frontal portion during 2016–2017 caused the thickening.

7. Conclusions

This study incorporates multi-source geodetic measurements to reveal the complex short-term variations in glacial mass. Signals extracted from both the east and up components of the GPS position time series and the GRACE-derived uplifts revealed that the bedrock near JI showed strong seasonal variations and three transient episodes: downward and eastward motion from late 2007 to early 2010, sustained upward and westward motion from 2010 to early 2013, and then downward and eastward motion till late 2016. Altimetry measurements first revealed the 2016 dynamic thickening in JI, which never happened in the past 2006–2015.

Our forward modeling of displacements from SMB and glacier dynamics together agree well with the extracted signals from GPS and GRACE. It shows that mass loss due to SMB was the dominant contributor to the short-term displacements in the past decade. Our modeling also shows that the mass loss from the upstream of fluxgate dominated the transient mass change, but the mass loss from downstream showed stronger seasonal variations.

The combined use of multi-source geodetic measurements and model data bring several benefits. Together, they provide sufficient cross-validations, make it possible to monitor the total ice mass change and partition the ice mass changes due to SMB, ice discharge, and calving front position changes, and provides different views to understand the highly-dynamic Jakobshavn Isbræ. Furthermore, this study provides an example of using multi-source geodetic data to investigate glaciers and can be potentially applied to other regions of Greenland, thus providing more means for monitoring and studying ongoing glacier changes.

Data availability. The GNET coordinate time series and ice elevation change rates data are provided by Shfaqat Abbas Khan at the National Space Institute, Technical University of Denmark (available at ftp://ftp.spacecenter.dk/pub/abbas/GNET/v1/). The GRACE GSM products (Release-06 Level-2) are provided by the Center for Space Research (CSR), University of Texas Austin (available at ftp://podaac.jpl.nasa.gov/allData/grace/L2/CSR/RL06/). The MAR SMB data are provided by Dr. Xavier Fettweis at Department of Geography, University of Liège (available at ftp://ftp.climato.be/fettweis/MARv3.5/Greenland/ERA_1958-2015_20km/monthly_outputs_interpolated_at_5km/). Ice flow velocity maps are provided by the National Snow and Ice Data Center (available at http://nsidc.org/data/NSIDC-0481 and http://nsidc.org/data/NSIDC-0646). The ice thickness maps are provided

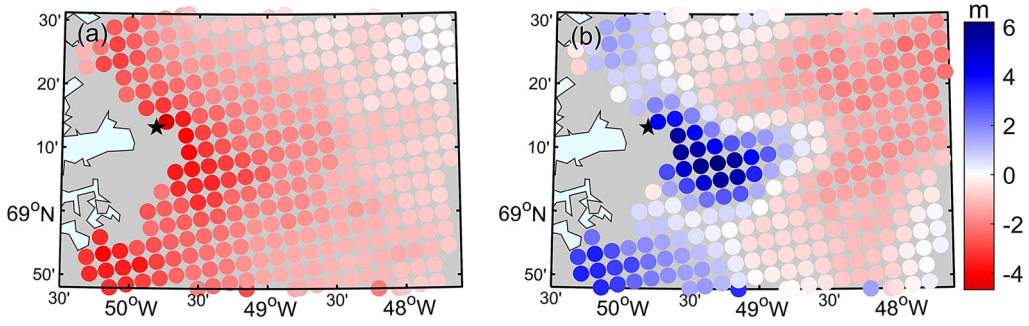

Fig. 8. Ice Elevation changes caused by SMB (a) and dynamics (b) from April 2016 to April 2017. The black star marks the location of KAGA.

by Mathieu Morlighem (available at http://sites.uci.edu/morlighem/dataproducts/bedmachine-greenland/). Calving front position data are provided by the Environmental Earth Observation Greenland Calving Front Dataset 1990–2016 (available at http://cryoportal.enveo.at).

Author contribution. The scientific analysis was jointly done by BZ, EZ, LL, and SAK. BZ analyzed the GPS and SMB data. EZ analyzed the glacier dynamics. LL provided important suggestions in this study. SAK provided the GPS coordinate time series and altimetry data. TvD provided the atmospheric and non-tidal ocean loading displacement data. LL provided the terrestrial water storage loading displacement data. BZ wrote this manuscript with contributions from LL and EZ. All authors helped revise and improve this manuscript. All authors have approved the final article.

Conflict of interest

The authors declare no conflict of interest.

Acknowledgements

We thank Dr. Xavier Fettweis for providing the MAR surface mass balance data, the Center for Space Research (CSR), University of Texas Austin for providing Level 2 GRACE data, and the UNAVCO Facility for providing GPS data, the National Snow and Ice Data Center for providing ice flow velocity maps, and Mathieu Morlighem for the ice thickness maps. Work at the Chinese University of Hong Kong was supported by Hong Kong Research Grants Council Grant CUHK24300414 and CUHK Direct Grant 3132764. S.A.K. was funded in part by Carlsbergfondet (grant CF14-0145) and the Danish Council for Independent Research (grant DFF-4181-00126). The Federal Ministry of Economics and Technology (grant 50EE1331 to V. Helm) has supported this work. Raw GPS data are available from the UNAVCO Facility with support from the National Science Foundation (NSF) and National Aeronautics and Space Administration (NASA) under NSF Cooperative Agreement No. EAR-0735156.

Appendix A. Supplementary material

Supplementary material related to this article can be found online at https://doi.org/10.1016/j.epsl.2018.09.029.

References

Adhikari, S., Ivins, E.R., Larour, E., 2017. Mass transport waves amplified by intense Greenland melt and detected in solid Earth deformation. Geophys. Res. Lett. 44 (10), 4965–4975.

Ahn, Y., Howat, I.M., 2011. Efficient automated glacier surface velocity measurement from repeat images using multi-image/multichip and null exclusion feature tracking. IEEE Trans. Geosci. Remote Sens. 49, 2838–2846. https://doi.org/10.1109/TGRS.2011.2114891.

Amundson, J.M., Truffer, M., 2010. A unifying framework for iceberg-calving models. J. Glaciol. 56, 822–830. https://doi.org/10.3189/002214310794457173.

Amundson, J.M., Truffer, M., Lüthi, M.P., Fahnestock, M., West, M., Motyka, R.J., 2008. Glacier, fjord, and seismic response to recent large calving events, Jakobshavn Isbræ, Greenland. Geophys. Res. Lett. 35 (22), L22501.

Bamber, J.L., Hardy, R.J., Joughin, I., 2000. An analysis of balance velocities over the Greenland ice sheet and comparison with synthetic aperture radar interferometry. J. Glaciol. 46 (152), 67–74.

Bevis, M., Wahr, J., Khan, S.A., Madsen, F.B., Brown, A., Willis, M., Kendrick, E., Knudsen, P., Box, J.E., van Dam, T., Caccamise II, D.J., Johns, B., Nylen, T., Abbott, R., White, S., Miner, J., Forsberg, R., Zhou, H., Wang, J., Wilson, T., Bromwich, D., Francis, O., 2012. Bedrock displacements in Greenland manifest ice mass variations, climate cycles and climate change. Proc. Natl. Acad. Sci. USA 109 (30), 11944.

Bondzio, J.H., Morlighem, M., Seroussi, H., Kleiner, T., Rückamp, M., Mouginot, J., Moon, T., Larour, E.Y., Humbert, A., 2017. The mechanisms behind Jakobshavn Isbræ's acceleration and mass loss: a 3D thermomechanical model study. Geophys. Res. Lett. 44. https://doi.org/10.1002/2017GL073309.

Cassotto, R., Fahnestock, M., Amundson, J.M., Truffer, M., Joughin, I., 2015. Seasonal and interannual variations in ice melange and its impact on terminus stability, Jakobshavn Isbræ, Greenland. J. Glaciol. 61, 76–88. https://doi.org/10.3189/2015JoG13J235.

Chen, Q., van Dam, T., Sneeuw, N., Collilieux, X., Weigelt, M., Rebischung, P., 2013. Singular spectrum analysis for modeling seasonal signals from GPS time series. J. Geodyn. 72, 25–35. https://doi.org/10.1016/j.jog.2013.05.005.

Cheng, M., Tapley, B.D., Ries, J.C., 2013. Deceleration in the Earth's oblateness. J. Geophys. Res., Solid Earth 118, 740–747. https://doi.org/10.1002/jgrb.50058.

Farrell, W.E., 1972. Deformation of the Earth by surface loads. Rev. Geophys. 10, 761–797. https://doi.org/10.1029/RG010i003p00761.

Fettweis, X., Box, J.E., Agosta, C., Amory, C., Kittel, C., Lang, C., van As, D., Machguth, H., Gallée, H., 2017. Reconstructions of the 1900–2015 Greenland ice sheet surface mass balance using the regional climate MAR model. Cryosphere 11, 1015. https://doi.org/10.5194/tc-11-1015-2017.

Ghil, M., Allen, M.R., Dettinger, M.D., Ide, K., Kondrashov, D., Mann, M.E., Robertson, A.W., Saunders, A., Tian, Y., Varadi, F., Yiou, P., 2002. Advanced spectral methods for climatic time series. Rev. Geophys. 40. https://doi.org/10.1029/2000RG000092.

Han, D., Wahr, J., 1995. The viscoelastic relaxation of a realistically stratified earth, and a further analysis of postglacial rebound. Geophys. J. Int. 120 (2), 287–311. https://doi.org/10.1111/j.1365-246X.1995.tb01819.x.

Helm, V., Humbert, A., Miller, H., 2014. Elevation and elevation change of Greenland and Antarctica derived from CryoSat-2. Cryosphere 8, 1539–1559. https://doi.org/10.5194/tc-8-1539-2014.

Holland, D.M., Thomas, R.H., De Young, B., Ribergaard, M.H., Lyberth, B., 2008. Acceleration of Jakobshavn Isbrae triggered by warm subsurface ocean waters. Nat. Geosci. 1, 659–664. https://doi.org/10.1038/ngeo316.

Howat, I.M., Ahn, Y., Joughin, I., van den Broeke, M.R., Lenaerts, J., Smith, B., 2011. Mass balance of Greenland's three largest outlet glaciers, 2000–2010. Geophys. Res. Lett. 38. https://doi.org/10.1029/2011GL047565.

Jeong, S., Howat, I.M., 2015. Performance of Landsat 8 Operational Land Imager for mapping ice sheet velocity. Remote Sens. Environ. 170, 90–101. https://doi.org/10.1016/j.rse.2015.08.023.

Jeong, S., Howat, I.M., Ahn, Y., 2017. Improved multiple matching method for observing glacier motion with repeat image feature tracking. IEEE Trans. Geosci. Remote Sens. 55, 2431–2441. https://doi.org/10.1109/tgrs.2016.2643699.

Joughin, I., Abdalati, W., Fahnestock, M., 2004. Large fluctuations in speed on Greenland's Jakobshavn Isbrae glacier. Nature 432, 608–610. https://doi.org/10.1038/nature03130.

Joughin, I., Smith, B.E., Howat, I.M., Scambos, T., Moon, T., 2010. Greenland flow variability from ice-sheet-wide velocity mapping. J. Glaciol. 56, 415–430. https://doi.org/10.3189/002214310792447342010.

Joughin, I., Smith, B.E., Howat, I.M., Floricioiu, D., Alley, R.B., Truffer, M., Fahnestock, M., 2012. Seasonal to decadal scale variations in the surface velocity of Jakobshavn Isbrae, Greenland: observation and model-based analysis. J. Geophys. Res., Earth Surf. 117. https://doi.org/10.1029/2011jf002110.

Joughin, I., Smith, B., Shean, D., Floricioiu, D., 2014. Brief communication: Further summer speedup of Jakobshavn Isbræ. Cryosphere 8, 209–214. https://doi.org/10.5194/tc-8-209-2014.

Khan, S.A., Liu, L., Wahr, J., Howat, I., Joughin, I., van Dam, T., Fleming, K., 2010a. GPS measurements of crustal uplift near Jakobshavn Isbræ due to glacial ice mass loss. J. Geophys. Res., Solid Earth 115. https://doi.org/10.1029/2010jb007490.

Khan, S.A., Wahr, J., Bevis, M., Velicogna, I., Kendrick, E., 2010b. Spread of ice mass loss into northwest Greenland observed by GRACE and GPS. Geophys. Res. Lett. 37. https://doi.org/10.1029/2010GL042460.

Khan, S.A., Sasgen, I., Bevis, M., van Dam, T., Bamber, J.L., Wahr, J., Willis, M., Kjær, K.H., Wouters, B., Helm, V., Csatho, B., Fleming, K., Bjørk, A.A., Aschwanden, A., Knudsen, P., Munneke, P.K., 2016. Geodetic measurements reveal similarities between post-Last Glacial Maximum and present-day mass loss from the Greenland ice sheet. Sci. Adv. 2. https://doi.org/10.1126/sciadv.1600931.

King, M.A., Altamimi, Z., Boehm, J., Bos, M., Dach, R., Elosegui, P., Fund, F., Hernández-Pajares, M., Lavallee, D., Cerveira, P.J.M., Penna, N., Riva, R.E.M., Steigenberger, P., van Dam, T., Vittuari, L., Williams, S., 2010. Improved constraints on models of glacial isostatic adjustment: a review of the contribution of ground-based geodetic observations. Surv. Geophys. 31, 465–507. https://doi.org/10.1007/s10712-010-9100-4465-507.

Kjeldsen, K.K., Khan, S.A., Bjørk, A.A., Nielsen, K., Mouginot, J., 2017. Ice-dammed lake drainage in west Greenland: drainage pattern and implications on ice flow and bedrock motion. Geophys. Res. Lett. 44 (14), 7320–7327.

Krabill, W., Abdalati, W., Frederick, E., Manizade, S., Martin, C., Sonntag, J., Swift, R., Thomas, R., Wright, W., Yungel, J., 2000. Greenland Ice Sheet: increased coastal thinning. Science 289, 428–430. https://doi.org/10.1029/2004gl021533.

Krabill, W.B., 2017. IceBridge ATM L2 Icessn Elevation, Slope, and Roughness [1993–2017]. NASA Distributed Active Archive Center at the National Snow and Ice Data Center, Boulder, Colorado, USA. http://nsidc.org/data/ilatm2.html.

Kuipers Munneke, P., Ligtenberg, S., Noël, B., Howat, I., Box, J., Mosley-Thompson, E., McConnell, J., Steffen, K., Harper, J., Das, S., van Den Broeke, M., 2015. Elevation change of the Greenland Ice Sheet due to surface mass balance and firn processes, 1960–2014. Cryosphere 9, 2009–2025. https://doi.org/10.5194/tc-9-2009-2015.

Liu, L., Khan, S.A., Dam, T., Ma, J.H.Y., Bevis, M., 2017. Annual variations in GPS-measured vertical displacements near Upernavik Isstrøm (Greenland) and contributions from surface mass loading. J. Geophys. Res., Solid Earth 122, 677–691. https://doi.org/10.1002/2016jb013494.

Morlighem, M., Williams, C.N., Rignot, E., An, L., Arndt, J.E., Bamber, J.L., Catania, G., Chauché, N., Dowdeswell, J.A., Dorschel, B., Fenty, I., Hogan, K., Howat, I., Hubbard, A., Jakobsson, M., Jordan, T.M., Kjeldsen, K.K., Millan, R., Mayer, L., Mouginot, J., Noël, B.P.Y., O'Cofaigh, C., Palmer, S., Rysgaard, S., Seroussi, H., Siegert, M.J., Slabon, P., Straneo, F., van den Broeke, M.R., Weinrebe, W., Wood, M., Zinglersen, K.B., 2017. BedMachine v3: complete bed topography and ocean bathymetry mapping of Greenland from multibeam echo sounding combined with mass conservation. Geophys. Res. Lett. 44. https://doi.org/10.1002/2017GL074954.

Muresan, I.S., Khan, S.A., Aschwanden, A., Khroulev, C., Van Dam, T., Bamber, J., van den Broeke, M.R., Wouters, B., Munneke, P.K., Kjær, K.H., 2016. Modelled glacier dynamics over the last quarter of a century at Jakobshavn Isbræ. Cryosphere 10, 597–611. https://doi.org/10.5194/tc-10-597-2016.

Nghiem, S.V., Hall, D.K., Mote, T.L., Tedesco, M., Albert, M.R., Keegan, K., Shuman, C.A., DiGirolamo, N.E., Neumann, G., 2012. The extreme melt across the Greenland ice sheet in 2012. Geophys. Res. Lett. 39. https://doi.org/10.1029/2012gl053611.

Nielsen, K., Khan, S.A., Spada, G., Wahr, J., Bevis, M., Liu, L., van Dam, T., 2013. Vertical and horizontal surface displacements near Jakobshavn Isbræ driven by melt-induced and dynamic ice loss. J. Geophys. Res., Solid Earth 118, 1837–1844. https://doi.org/10.1002/jgrb.50145.

Rangelova, E., Van der Wal, W., Sideris, M.G., Wu, P., 2010. Spatiotemporal analysis of the GRACE-derived mass variations in North America by means of multi-channel singular spectrum analysis. In: Gravity, Geoid and Earth Observation. Springer, Berlin, Heidelberg, Germany, pp. 539–546.

Rangelova, E., Sideris, M.G., Kim, J.W., 2012. On the capabilities of the multi-channel singular spectrum method for extracting the main periodic and non-periodic variability from weekly GRACE data. J. Geodyn. 54, 64–78. https://doi.org/10.1016/j.jog.2011.10.006.

Rignot, E., Kanagaratnam, P., 2006. Changes in the velocity structure of the Greenland Ice Sheet. Science 311, 986–990. https://doi.org/10.1126/science.1121381.

Rignot, E., Box, J.E., Burgess, E., Hanna, E., 2008. Mass balance of the Greenland ice sheet from 1958 to 2007. Geophys. Res. Lett. 35 (20).

Rodell, M., Houser, P.R., Jambor, U., Gottschalck, J., Mitchell, K., Meng, C.-J., Arsenault, K., Cosgrove, B., Radakovich, J., Bosilovich, M., Entin, J.K., Walker, J.P., Lohmann, D., Toll, D., 2004. The global land data assimilation system. Bull. Am. Meteorol. Soc. 85, 381–394. https://doi.org/10.1175/BAMS-85-3-381.

Swenson, S., Chambers, D., Wahr, J., 2008. Estimating geocenter variations from a combination of GRACE and ocean model output. J. Geophys. Res. 113. https://doi.org/10.1029/2007JB005338. B08410.

Tedesco, M., Fettweis, X., Van den Broeke, M.R., Van de Wal, R.S.W., Smeets, C.J.P.P., van de Berg, W.J., Serreze, M.C., Box, J.E., 2011. The role of albedo and accumulation in the 2010 melting record in Greenland. Environ. Res. Lett. 6. https://doi.org/10.1088/1748-9326/6/1/014005.

Thomas, R.H., Abdalati, W., Frederick, E., Krabill, W.B., Manizade, S., Steffen, K., 2003. Investigation of surface melting and dynamic thinning on Jakobshavn Isbræ, Greenland. J. Glaciol. 49, 231–239. https://doi.org/10.3189/172756503781830764.

van Dam, T., Wahr, J., Lavallée, D., 2007. A comparison of annual vertical crustal displacements from GPS and Gravity Recovery and Climate Experiment (GRACE) over Europe. J. Geophys. Res. 112, B03404. https://doi.org/10.1029/2006JB004335.

Walwer, D., Calais, E., Ghil, M., 2016. Data-adaptive detection of transient deformation in geodetic networks. J. Geophys. Res., Solid Earth 121, 2129–2152. https://doi.org/10.1002/2015jb012424.

Wahr, J., Khan, S.A., Dam, T., Liu, L., Angelen, J.H., Broeke, M.R., Meertens, C.M., 2013. The use of GPS horizontals for loading studies, with applications to northern California and southeast Greenland. J. Geophys. Res., Solid Earth 118 (4), 1795–1806. https://doi.org/10.1002/jgrb.50104.

Zhang, B., Liu, L., Khan, S.A., van Dam, T., Zhang, E., Yao, Y., 2017. Transient variations in glacial mass near Upernavik Isstrøm (west Greenland) detected by the combined use of GPS and GRACE data. J. Geophys. Res., Solid Earth 122. https://doi.org/10.1002/2017jb014529.

Zwally, H.J., Schutz, R., Bentley, C., Bufton, J., Herring, T., Minster, J., Spinhirne, J., Thomas, R., 2012. GLAS/ICESat L2 Antarctic and Greenland Ice Sheet Altimetry Data V031. NASA Distributed Active Archive Center at the National Snow and Ice Data Center, Digital Media, Boulder, Colorado.